

# NUMERICAL SIMULATION OF SELF-PROPELLED FLYING OF A THREE-DIMENSIONAL BIRD WITH FLAPPING WINGS<sup>†</sup>

WU Chui-Jie\* , ZHU Lin-Lin

State Key Laboratory of Structural Analysis for Industrial Equipment,  
School of Aeronautics and Astronautics, Dalian University of Technology,  
Dalian 116024

**Keywords:** *self-propelled, bird flying, numerical simulation, three-dimensional*

## Abstract

*The numerical simulation and control of three-dimensional bionic bird's self-propelled flying in a viscous flow and the mechanics of bird flying are carried out in this study. The bird is propelled and lifted by flapping and rotating wings. The best flying of the bird is achieved by adjusting the flapping period, flapping amplitude, maximum rotation angle of wings, rotation angle velocity of wings, and density ratio. Both the thrust and lift of the bionic bird are increased with the decrease of the flapping period or the increase of the flapping amplitude, and the bird can fly faster forward when the flapping period is shorter and upward when the flapping amplitude is larger, which is found in this study. A three-dimensional computational fluid dynamics package, which includes the immersed boundary method and the volume of fluid method, the adaptive multi-grid finite volume method, and the swimming and flying control strategy is used in this study.*

## 1 Introduction

In the nature, many animals are capable of controlling the flow using an active or passive deformation of the body surface, moreover they have better movement performance than the man-made vehicles. Their special motion can reduce

the drag force, suppress the turbulence and produce much more lift than the human understanding as a credible method of turbulent flow control. Most birds are much more efficient flyers than the man-made vehicles, and the flapping flight is more complicated than the flight with fixed wings, as its dynamics is determined not only by its deformation but also by its wing motion aspects, such as plunge, pitch, and rotational phase difference between the plunge and pitch. Understanding the dynamic interaction between the fluid and the deformable wing may lead to a better micro air vehicles MAV design[1].

In recent years, much work has been done on the flapping flight using both experimental and computational methods (e.g. Ellington[2], Dickinson[3], Sane and Dickinson[4], Liu[5], Sun and Tang[6, 7], Usherwood and Ellington[8], Wang[9]), also a considerable understanding of the aerodynamic force generation mechanism has been achieved. However, in most of these studies, the flight was fixed and the body couldn't move or rotate freely when is subjected to the action of the pressure, the viscous force and the gravity. What happen if the flapping flight with the flapping and rotating wings is unfixed? Study of a three-dimensional bird's self-propelled flying is more similar to the real flyer in the nature than the fixed studies.

Pennycuick[10] has collected wingbeat frequencies of 15 species of birds cruising flight, observed in the field in level. An equation about the relationship between the gravity and the flapping frequency was found, the gravity

\*Corresponding author (email: cjwudut@dlut.edu.cn)

<sup>†</sup>Supported by National Natural Science Foundation of China (No. 11072053, 11372068)

is proportional to the flapping frequency, so the lift is proportional to the flapping frequency, too. Salman A. Ansari, Kevin Knowles, and Rafal Zbikowski[11] studied the effects of wing kinematics on the aerodynamic performances of insect-like flapping wings in hover based on non-linear unsteady aerodynamic models. They found that the lift and the thrust increased with increasing flapping frequency, flapping amplitude, and advanced wing rotation, but such increases were limited by practical conditions. In this study, the thrust and lift of the bionic bird has been investigated with variable flapping frequency and flapping amplitude using a three-dimensional self-propelled flying bird.

In the present study, the numerical simulation of three-dimensional bionic bird is a convenient tool. This is achieved by a CFD software package for 3D moving boundary problems, which combines the adaptive mesh refinement method, the immersed boundary method and the volume of fluid (VOF) methods. It has advantages of greatly saving the computing time and accurately portraying the three-dimensional moving boundary. Based on the boundary vorticity-flux (BVF) theory proposed by Wu[12], the original integrand of overall performance parameters (i.e. forces and moment of the flow) is transformed to the moments of its spatial derivatives, thus revealing the effect of various local dynamic processes on the integrated performance and tracing the underlying fluid physical sources to the moving body surface. The computations of the forces exerted on the bird body and the relationship between the forces and vortex structures are carried out by the BVF theory in 3D bionic bird's self-flying.

## 2 Numerical approaches

### 2.1 Governing equations and numerical method

In this study, the governing incompressible unsteady Navier-Stokes equations are solved using the finite volume method. The Cartesian adaptive mesh refinement technique is used to compute the flows with minimum overhead. The computational domain is spatially discretized by using a

cubic finite volumes organized hierarchically as an octree. The projection and the multi-levels methods are used to solve the Poisson equation of pressure. The convective terms are discretized by using the second order Godunov type scheme. The diffusion terms are discretized with the implicit Crank-Nicolson scheme, which can eliminate the viscous stability constraint. The detail of the numerical algorithms refers to [13].

### 2.2 Adaptive moving boundaries with the Ghost-cell immersed boundary method

The study of bird self-propelled flying is a moving boundaries problem involving complex geometry. The computing methods of moving boundaries problem are usually classified into the body-fitted moving mesh method and immersed boundary method (IBM) for computational fluid dynamics. The boundary conditions can be simply and accurately set using body-fitted moving mesh method, but the grid generation is a difficult and time-consuming task. The immersed boundary method requires significantly less computation than other methods without sacrificing the accuracy. In the present study, moving boundaries are treated with ghost-cell IBM, which employs discrete forcing where the forcing is either implicitly or explicitly applied to the discretized Navier-Stokes equations. The technique of adaptive multi-grids is used and the adaptive refinement criteria are both vorticity and  $\nabla T$ , where  $T$  is a tracer of VOF. This ensures that the meshes intersecting with the moving body boundaries are the finest and accurate representation of moving boundaries is achieved[3].

## 3 Motion equations and flying parameters

### 3.1 Motion equations

The dynamics equations for the self-propelled three-dimensional bird are

$$m \frac{d\mathbf{u}}{dt} = \mathbf{F}, \quad \frac{d\mathbf{L}}{dt} = \mathbf{M}, \quad (1)$$

$$\mathbf{F} = - \int_{\partial B} (-p\mathbf{n} + \mu\boldsymbol{\omega} \times \mathbf{n}) ds, \quad (2)$$

$$\mathbf{F} = - \int_{\partial B} \rho x \times \left( \frac{1}{2} \boldsymbol{\sigma}_p + \boldsymbol{\sigma}_{vis} \right) ds \quad (3)$$

where  $m$  is the mass of the bionic bird;  $\mathbf{u}$  is the velocity vector;  $\mathbf{F}$  is the aerodynamic force;  $\mathbf{M}$  is the moment and  $\mathbf{L}$  is the moment of momentum;  $\partial B$  is the three-dimensional bionic bird surface,  $\mathbf{n}$  is the unit normal vector pointing out of the bird body surface;  $\rho$ ,  $\mu$ ,  $\omega$  are the air density, shear viscosity and vorticity, respectively;  $\sigma_p = \mathbf{n} \times \nabla \mathbf{p} / \rho$ ,  $\sigma_{vis} = \mathbf{v}(\mathbf{n} \times \nabla) \times \omega$  are the boundary vorticity flux caused by the tangential pressure gradient and the viscous vortical effect, respectively. Eq.(3) is a force expression of the boundary vorticity flux while Eq.(2) is a classical force formula derived directly from the momentum balance [12].

In the study, two sets of coordinates are used, which are the bird body coordinates  $(x_l, y_l, z_l)$  and the global coordinates  $(x, y, z)$ . Two sets of coordinates can be converted to each other.

### 3.2 The flapping rule and kinematic parameters

The bird body consists of four parts: the body trunk, the tail and two flapping wings. The three-dimensional profile of the bird is shown in Fig.1, which are observed from the side and above, respectively.

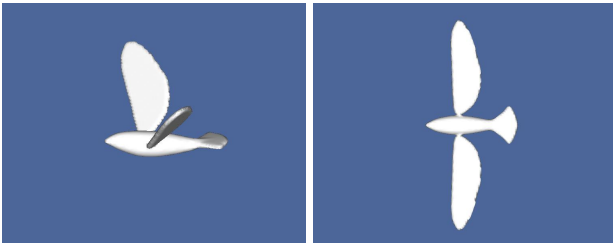


Fig. 1 . 3D profile of the bird body.

The flapping motion of the wings contains two steps: rotation and flapping. The first step, both wings rotate along the  $y$  axis with the same angle, the rotation angle  $\alpha 2(t)$  is shown in Eq.(5). The second step, both wings rotate along two straight lines parallel to the  $x$  axis, the two lines contain the points  $(x_p, y_p, z_p)$  and  $(x_p, -y_p, z_p)$ , respectively, which are intersection point of the bird body and each of the wings; the flapping angle of the right wing is always reversed to the left one. In this study, the flapping angle of the left

wing  $\alpha 1(t)$  is defined as the major one, which is shown in Eq.(4).

In the bird body coordinate system, the flapping angle  $\alpha 1(t)$  and the rotation angle  $\alpha 2(t)$  in the first period can be written as:

$$\alpha 1(t) = \alpha_m \times \sin\left(\frac{2\pi t}{T} - \frac{\pi}{2}\right) \quad (4)$$

$$\alpha 2(t) =$$

$$\left\{ \begin{array}{ll} \alpha_n \times \sin\left(\frac{\pi t}{2T_1}\right), & (0 \leq t < T_1) \\ \alpha_n, & (T_1 \leq t \leq \frac{T}{2} - T_1) \\ \alpha_n \times \sin\left[\left(\frac{T}{2} - t\right) \times \frac{\pi}{2T_1}\right], & (\frac{T}{2} - T_1 < t < \frac{T}{2} + T_1) \\ -\alpha_n, & (\frac{T}{2} + T_1 \leq t \leq T - T_1) \\ \alpha_n \times \sin\left[(t - T) \times \frac{\pi}{2T_1}\right], & (T - T_1 < t < T) \end{array} \right. \quad (5)$$

Where  $t$  is the time,  $\alpha_m$  is the maximum flapping angle of the wings,  $\alpha_n$  is the maximum rotation angle of the wings,  $T$  is the flapping period,  $T_1$  is used to control the rotation time of the wings at the beginning and the end of the stroke.

The Eq.(4) is presented by the red real line with " $\Delta$ " in Fig.2.(a), which is part of the sine function with maximum value  $\alpha_m$  and minimum value  $-\alpha_m$ . The Eq.(5) is presented by the blue real line with " $\circ$ " in Fig.2.(a), more details are presented in Fig.2.(b). The first equation presents the left black dashed line, which is part of the sine function, where 0 and  $\alpha_n$  are the minimum and maximum value of the line, and  $T_1$  is the maximum  $x$  axis value. The second equation presents the left red real line, which is a straight line with a constant value  $\alpha_n$ . The third equation presents the dark blue dash dot line, which is part of the sine function, where  $\alpha_n$  and  $-\alpha_n$  are the maximum and minimum values of the line. The fourth equation presents the right red real line, which is a straight line with a constant value  $-\alpha_n$ . The fifth equation presents the right black dashed line, which is part of the sine function, where  $-\alpha_n$  and 0 are the minimum and maximum value of the

line. In Fig.2.(a),  $\alpha_m = 40^\circ$ ,  $\alpha_n = 35^\circ$ ,  $T = 0.02$ ,  $T_1 = T/10 = 0.002$ .

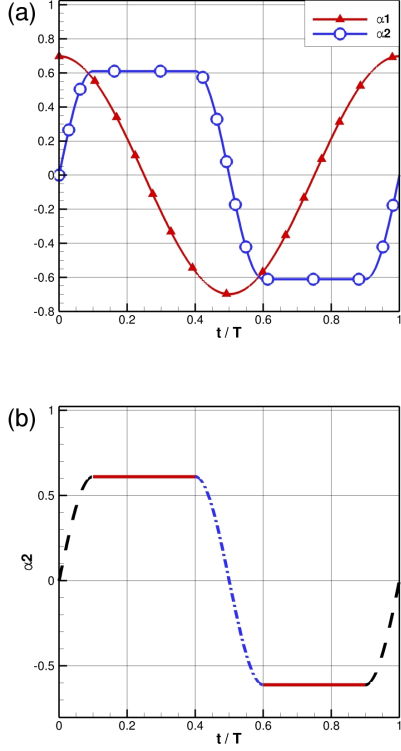


**Fig. 2** . The angle of the flapping wings. (a)The flapping angle and rotation angle in one period; (b)The rotation angle in one period.

Downstroke of one period consists of four parts: pitching-down rotation and translational acceleration at the beginning of the stroke, constant rotation angle and translational acceleration, constant rotation angle and translational deceleration, and pitching-up rotation and translational deceleration at the end of the stroke. Upstroke of the period consists of the other four parts: pitching-up rotation and translational acceleration at the beginning of the stroke, constant rotation angle and translational acceleration, constant rotation angle and translational deceleration, and pitching-down rotation and translational deceleration at the end of the stroke. All above are shown in Fig.2.(a).

### 3.3 Boundary and initial conditions

All boundaries of the computational region are set to be no slip boundary conditions, i.e.

$$u_b = v_b = w_b = 0.$$

So the computational region is like a flume without inflow nor outflow.

The initial condition is

$$u = v = w = 0.$$

The immersed boundary conditions on the bird's body surface are as follows. The body surface velocity of every point consists of the following three components.

(1)The velocity  $\mathbf{V}_0$  arose from the aerodynamic force.

$$\mathbf{V}_0 = u_0\mathbf{i} + v_0\mathbf{j} + w_0\mathbf{k}$$

(2)The linear velocity  $\mathbf{V}_r$  arose from the rotation.

$$\mathbf{V}_r = \boldsymbol{\omega} \times (\mathbf{x} - \mathbf{x}_0) \quad (6)$$

Where  $\mathbf{x}$  is the coordinate of a point on the body surface,  $\mathbf{x}_0$  is the coordinates of the gravity centre, which is computed at every time step.

(3)The velocity  $\mathbf{V}_f$  arose from the flapping motion, which contains flapping and rotation. First, the velocity arose from the flapping is:

$$\begin{cases} u_1 = 0, \\ v_1 = \theta_1 z_1, \\ w_1 = -\theta_1 y_1. \end{cases}$$

Where,  $\theta_1$  is the angle velocity along the straight line parallel to the  $x$  axis.  $(x_1, y_1, z_1)$  and  $\theta_1$  is defined as follow:

$$\begin{cases} x_1 = x_l - x_p, \\ y_1 = y_l - y_p, \\ z_1 = z_l - z_p, \end{cases} \quad \theta_1 = \frac{d[\alpha_1(t)]}{dt}.$$

Where,  $(x_l, y_l, z_l)$  is the bird body coordinates,  $(x_p, y_p, z_p)$  is the intersection point of the body trunk with one of wings.

Second, the velocity arose from the rotation is:

$$\begin{cases} u_2 = -\theta_2 z_2, \\ v_2 = -\theta_2 x_2 \times \sin(\alpha_1), \\ w_2 = \theta_2 x_2 \times \cos(\alpha_1). \end{cases}$$

Where,

$$\begin{cases} x_2 = x_1, \\ y_2 = y_1 \cos(-\alpha 1) - z_1 \sin(-\alpha 1), \\ z_2 = y_1 \sin(-\alpha 1) + z_1 \cos(-\alpha 1), \\ \theta_2 = \frac{d[\alpha 2(t)]}{dt}. \end{cases}$$

The velocity  $\mathbf{V}_{lf}$  generated by the flapping motion in bird body coordinates is:

$$\mathbf{V}_{lf} = \begin{pmatrix} u_{fl} \\ v_{fl} \\ w_{fl} \end{pmatrix}, \quad \begin{cases} u_{lf} = u_1 + u_2, \\ v_{lf} = v_1 + v_2, \\ w_{lf} = w_1 + w_2. \end{cases}$$

As we know:

$$m \frac{d\mathbf{L}}{dt} = \mathbf{M}, \quad \mathbf{L} = \mathbf{I} \cdot \boldsymbol{\Omega}.$$

Where:  $\boldsymbol{\Omega} = (\omega_1, \omega_2, \omega_3)^T$  is the angular velocity of the three-dimensional bird,  $\mathbf{I}$  is the inertia tensor:

$$\begin{pmatrix} \sum(y_i^2 + z_i^2)m_i & -\sum(x_i y_i)m_i & -\sum(x_i z_i)m_i \\ -\sum(x_i y_i)m_i & \sum(x_i^2 + z_i^2)m_i & -\sum(y_i z_i)m_i \\ -\sum(x_i z_i)m_i & -\sum(y_i z_i)m_i & \sum(x_i^2 + y_i^2)m_i \end{pmatrix}$$

Based on all above, we can achieve  $\boldsymbol{\Omega}$  and the transition matrix  $\mathbf{A}$  from bird body coordinates  $(x_l, y_l, z_l)$  to the global coordinates  $(x, y, z)$ .

$$\mathbf{A} = \begin{pmatrix} 1 & -\Delta t \omega_3 & \Delta t \omega_2 \\ \Delta t \omega_3 & 1 & -\Delta t \omega_1 \\ -\Delta t \omega_2 & \Delta t \omega_1 & 1 \end{pmatrix}$$

So the boundary velocity generated by the flapping motion in the global coordinate system is:

$$\mathbf{V}_f = \mathbf{A} \cdot \mathbf{V}_{fl}$$

In the local body coordinate system, the velocity of the bird wings generated by the flapping wings is:

$$\begin{cases} u_b = u_0 + u_r + u_f \\ v_b = v_0 + v_r + v_f \\ w_b = w_0 + w_r + w_f \end{cases}$$

## 4 Results and analysis

In this paper, the dimensionless bird's two wings total length is 1. The computational domain is  $6 \times 3 \times 3$  (length  $\times$  width  $\times$  height). The kinematics viscosity coefficient of the fluid is  $\nu = 15.7 \times 10^{-6}$ .

In this study, the body trunk and two flapping wings are rigid body. At the beginning, the bird is fixed, we control the wings' flapping and rotation, so we can achieve the velocity of every point on the bird surface, which we used as immersed boundary condition; then we can use the Navier-Stokes solver to compute the viscous force and the pressure force with the immersed boundary condition and the computational region boundary condition. Base on all above, the resulting force from the gravity, viscous force and pressure force can be achieved. In the end, we achieve the new flight position including the translation and rotation from the last position. The next step is to use this translation velocity and rotation angle velocity getting the velocity of every point on the bird surface as new immersed boundary condition.

### 4.1 Flying velocity and forces exerted on the bird body

From Fig.3.(a), it can be seen that all the forces on the bird changes periodically, the period is the same as the flapping cycle of the bird wings, where the period is  $T = 0.02$ , and in the first  $1/4$  period the bird was fixed (only wings flapping and rotating without body translating nor rotating). In Fig.3.(a),  $F_x$  is the thrust along the  $x$  axis,  $F_y$  is the force along the  $y$  axis, which makes bird turn left or right in  $x - y$  plane,  $F_z$  is the lift along the  $z$  axis. Fig.3.(a) also shows that,  $F_x$  is almost positive at the beginning, later decreases gradually with the increase of the velocity  $u$  along the  $x$  axis, and the velocity  $u$  increases all the time, which is shown in Fig.3.(b).  $F_y$  is almost zero, so the velocity  $v$  is almost zero. In the first  $T/2$  of a period when the wings flap down, the lift  $F_z$  is positive, and the upward velocity increases gradually which is shown in Fig.3.(b), and in the last  $T/2$  of the period when the wings flap upon, the lift  $F_z$  is negative, the upward velocity decreases gradually, which we can see clearly in Fig.3.(b), too. In this study, the bird has initial velocity  $u = v = w = 0$ .

Based on all above, we can see that in Fig.3.(c), in the  $x - y$  plane, the moving path (the green real line) is almost a straight line, in  $x - z$  plane, the flight height (the dark blue real line) changed periodically

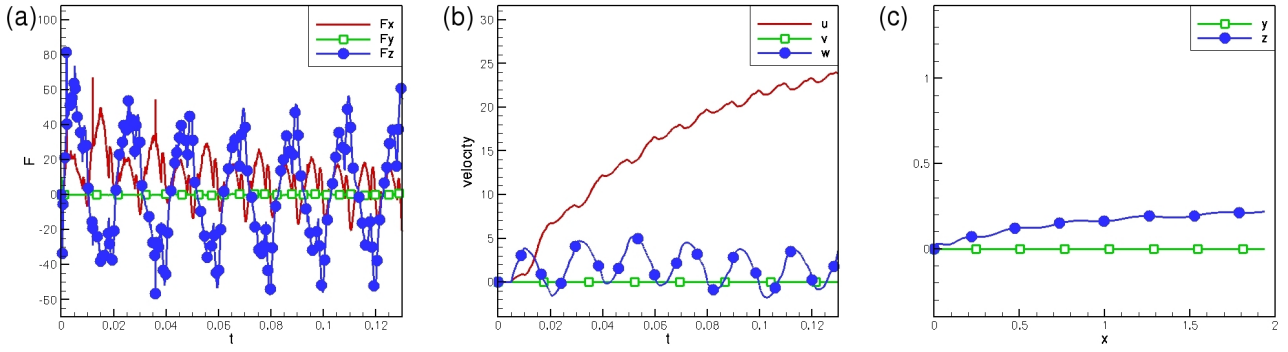


**Fig. 3** . (a)The force, (b)velocity and (c)flying path of the bird.

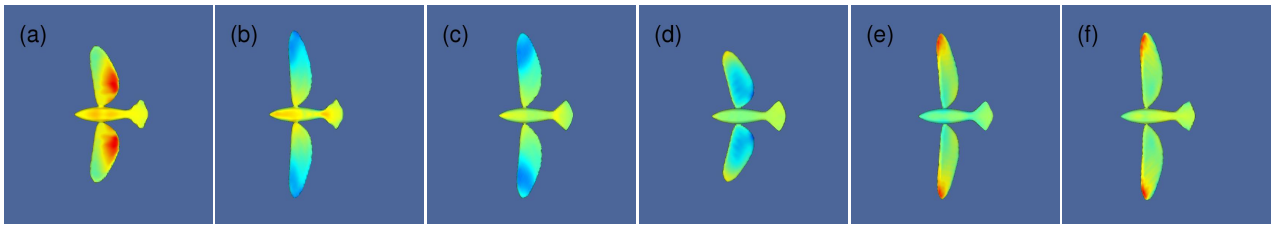


**Fig. 4** . Pressure distribution on the upper surface during the flapping in a period. (a)  $t/T = 0$ , (b)  $t/T = 0.2$ , (c)  $t/T = 0.3$ , (d)  $t/T = 0.5$ , (e)  $t/T = 0.7$ , (f)  $t/T = 0.8$ .

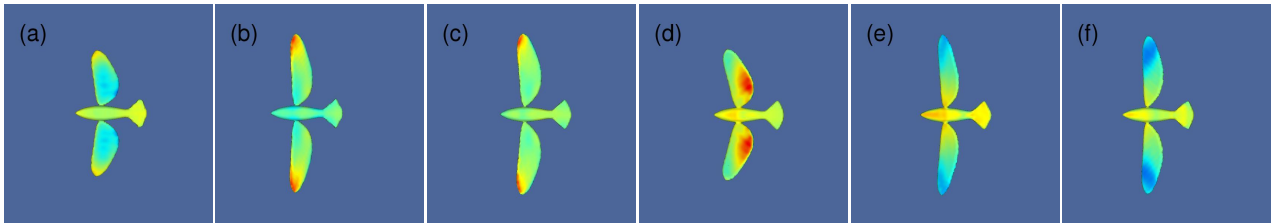


**Fig. 5** . Pressure distribution on the lower surface during the flapping in a period. (a)  $t/T = 0$ , (b)  $t/T = 0.2$ , (c)  $t/T = 0.3$ , (d)  $t/T = 0.5$ , (e)  $t/T = 0.7$ , (f)  $t/T = 0.8$ .

and increased gradually, which begins from  $(0.0, 0.0)$  and ends to  $(1.94, 0.22)$ , so it keeps upward, which is well-matched in the force and velocity.

Fig.4 and Fig.5 shows the pressure distribution on the upper and lower surface of the bird at different moments in one period. In Fig.4.(a) and Fig.5.(a),  $t = 0$ , the flapping angle of the wings is maximum, and the wings' tip is at the top of the path, when the flapping speed is 0 and the rotation angle velocity is maximum. In Fig.4.(b) and Fig.5.(b),  $t = 0.2T$ , both flapping angle and rotation angle of the wings is positive, when the flapping speed is increasing and the rotation angle velocity is 0. In Fig.4.(c) and Fig.5.(c),  $t = 0.3T$ , the flapping angle of the wings is negative, and the rotation angle is positive, when the flapping speed is

decreasing and the rotation angle velocity is 0. In Fig.4.(d) and Fig.5.(d),  $t = 0.5T$ , the flapping angle of the wings is in negative maximum, and the wings' tip is at the bottom of the path, when the flapping speed is 0 and the rotation angle velocity is in negative maximum. In Fig.4.(e) and Fig.5.(e),  $t = 0.7T$ , both flapping angle and rotation angle of the wings is negative, when the flapping speed is increasing and the rotation angle velocity is 0. In Fig.4.(f) and Fig.5.(f),  $t = 0.8T$ , the flapping angle of the wings is positive, and the rotation angle is negative, when the flapping speed is decreasing and the rotation angle velocity is 0.

Fig.6 shows the three-dimensional structures due the bird's self-propelled flying, which is observed from the side and above.

## Numerical simulation of self-propelled flying of a three-dimensional bird with flapping wings

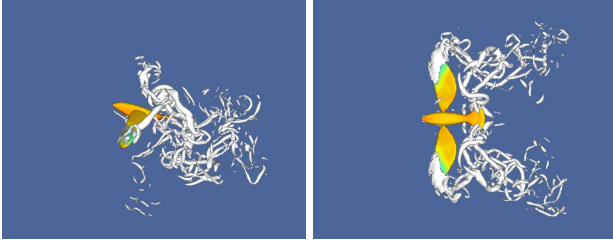


Fig. 6 . 3D vortex structure.

### 4.2 Different flapping period compared

In the present study, three flapping period  $T = 0.03, 0.02, 0.01$  was studied, which is shown in Fig.7.

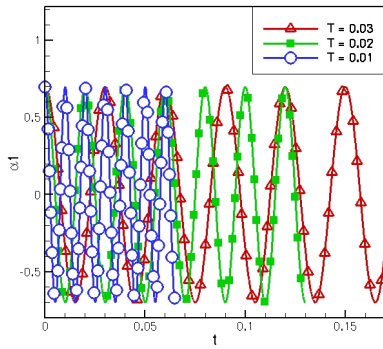
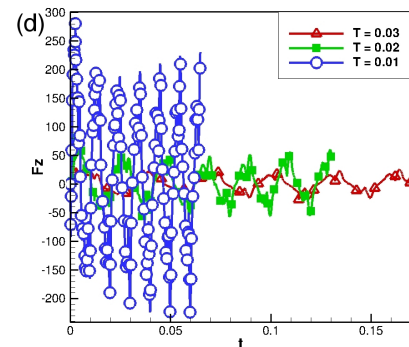
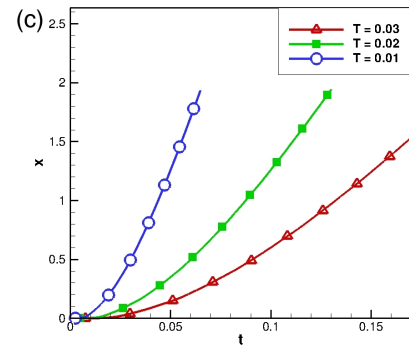
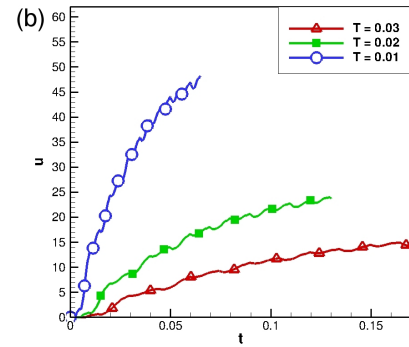
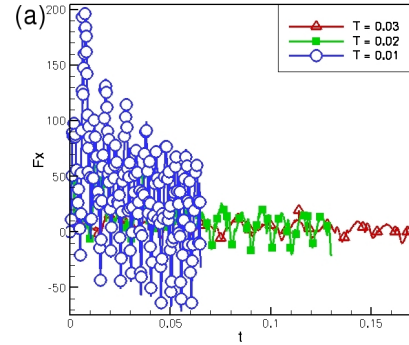


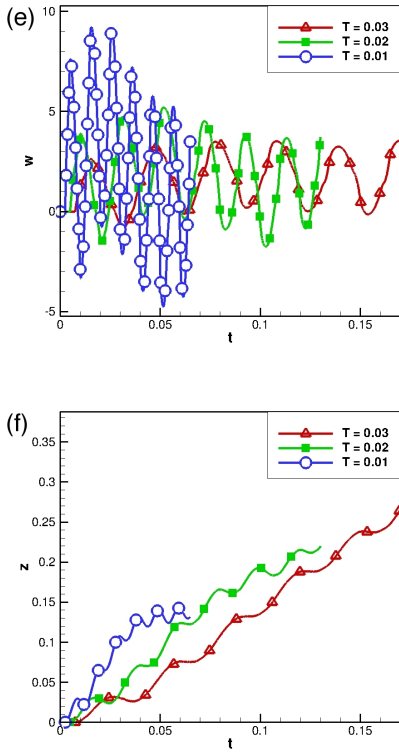
Fig. 7 . Different flapping period.

Fig.8.(a) shows that the thrust changes periodically, the period is the same as the flapping cycle of the wings. One can see that the thrust sometimes is positive sometimes is negative, but it is always increases with the decrease of the flapping period. Fig.8.(b) and Fig.8.(c) shows that the velocity and the displacement of the body along the  $x$  axis is increased with the decrease of the flapping period, too, which is well-matched in the force. Fig.8.(d) shows that the lift changes periodically when the flapping period is equal to the three values. We found that the lift on the bird usually increases with the decrease of the flapping period. Fig.8.(e) and Fig.8.(f) shows that the velocity and the displacement of the bird along the  $z$  axis is increased with the decrease of the flapping period, too.

Both the velocity and displacement of the bird along the  $x$  axis and the  $z$  axis are increased with the decrease of the flapping period, but the velocity and displacement along the  $x$  axis is increased faster, so the flight height of flying path in the  $x - z$  plane increase slower with the decrease of the flapping period,

which is shown in Fig.9. So, the bird can fly faster forward if the flapping period is shorter.





**Fig. 8** . Different flapping period compared. (a) the thrust, (b) the velocity  $u$ , (c) the displacement  $x$ , (d) the lift, (e) the velocity  $w$ , (f) the displacement  $z$ .

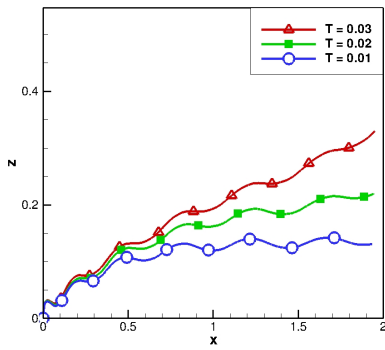
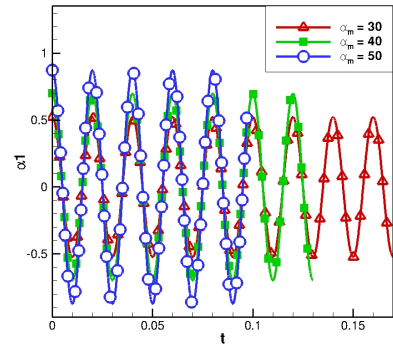


**Fig. 9** . Path of different flapping period.

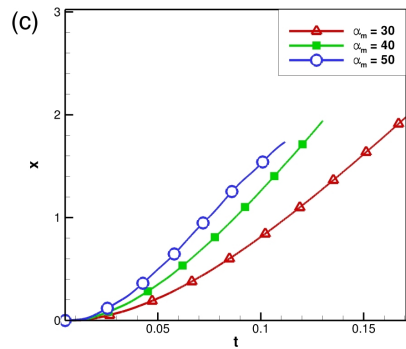
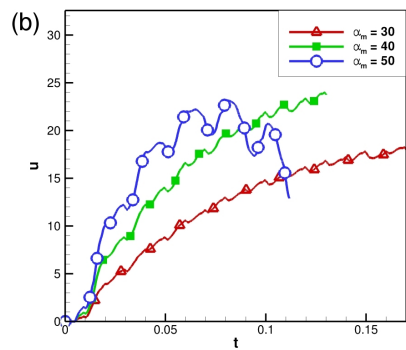
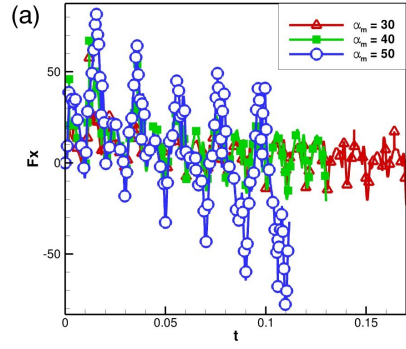
### 4.3 Different flapping amplitude compared

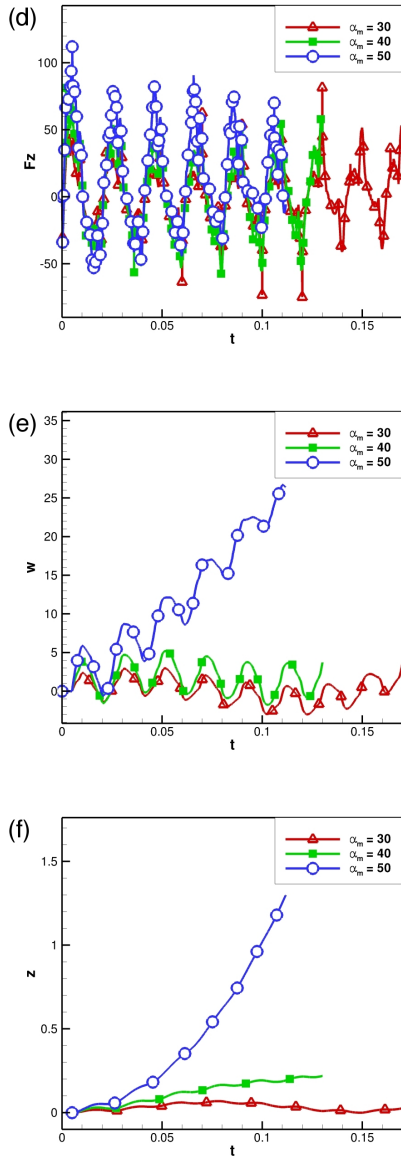
In this present study, three flapping amplitude (the degree of angle)  $\alpha_m = 30^\circ, 40^\circ, 50^\circ$  was studied, which is shown in Fig.10.

Fig.11.(a) shows that the thrust changes periodically, the period is the same as the flapping cycle of the wings. One can see that the thrust is always increases



**Fig. 10** . Different flapping amplitude.





**Fig. 11** . Different flapping amplitude compared. (a) the thrust, (b) the velocity  $u$ , (c) the displacement  $x$ , (d) the lift, (e) the velocity  $w$ , (f) the displacement  $z$ .

with the increase of the flapping amplitude. Fig.11.(b) and Fig.11.(c) shows that the velocity and the displacement of the bird along the  $x$  axis is increased with the increase of the flapping amplitude, too, which is well-matched in the force. Fig.11.(d) shows that the lift changes periodically when the flapping amplitude is equal to the three values. We found that the lift on the bird usually increases with the increase of the flapping amplitude. Fig.11.(e) and Fig.11.(f) shows that the velocity and the displacement of the bird along

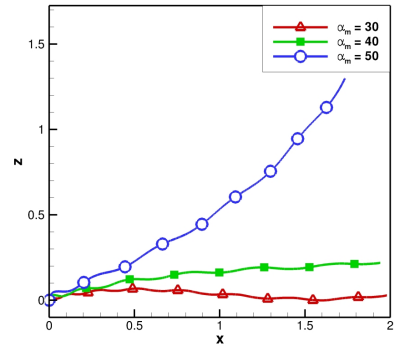


**Fig. 12** . Path of different flapping period.

the  $z$  axis is increased with the increase of the flapping amplitude, too.

Both the velocity and displacement of the bird along the  $x$  axis and the  $z$  axis are increased with the increase of the flapping amplitude, but the velocity and displacement along the  $z$  axis is increased faster, so the flight height of flying path in the  $x - z$  plane increase faster with the increase of the flapping amplitude, which is shown in Fig.12. So, the bird can fly faster upward if the flapping amplitude is larger.

## 5 Conclusion

In the numerical simulations and vorticity dynamics of the three-dimensional bionic birds self-propelled flying in a viscous flow, the lift and thrust are produced by the flapping wings, which contains flapping and rotation. Flapping and rotation play different roles at different moments of one period. In this study, different flapping period was studied, both the lift and thrust are increased with the decrease of the flapping period, but the thrust is increased faster. So, the bird can fly faster forward if the flapping period is shorter. Different flapping amplitude was studied, too, both the lift and thrust are increased with the increase of the flapping amplitude, but the lift is increased faster. So, the bird can fly faster upward if the flapping amplitude is larger.

Flapping period plays a big role in the velocity  $u$  along the  $x$  axis, and flapping amplitude plays a big role in the velocity  $w$  along the  $z$  axis. So, reduce the flapping period, the bird will fly faster forward, increase the flapping amplitude, the bird will fly faster upward.

## References

- [1] Shyy W, Lian Y, Tang J, Viieru D, Liu H. *Aerodynamics of Low Reynolds Number flyers*. Cambridge University Press, New York, 2008.
- [2] Ellington C P, Van Den Berg C, Willmott A P, Thomas A L R. *Leading-edge vortices in insect flight*. *Nature*, 1996, 384: 626-630.
- [3] Dickinson M H, Lehmann F O, Sane S P. *Wing rotation and the aerodynamic basis of insect flight*. *Nature*, 1999, 284: 1954-1960.
- [4] Sane S P, Dickinson M H. The control of flight force a flapping wing. *lift and drag production*. *J Exp Biol*, 2001, 204: 2607-2626.
- [5] Liu H, Ellington C P, Kawachi K, Van Den Berg C, Willmott A P. *A computational fluid dynamic study of hawkmoth hovering*. *J Exp Biol*, 1998, 201: 461-477.
- [6] Sun M, Tang J. *Unsteady aerodynamic force generation by a model fruit fly wing in flapping motion*. *J Exp Biol*, 2002a, 205: 55-70.
- [7] Sun M, Tang J. *Lift and power requirements of hovering flight in Drosophila virilis*. *J Exp Biol*, 2002b, 205: 2413-2427.
- [8] Usherwood J R, Ellington C P. The aerodynamics of revolving wings. II. *Propeller force coefficients from mayfly to quail*. *J Exp Biol*, 2002, 205: 1565-1576.
- [9] Wang Z J, Birch J M, Dickinson M H. Unsteady forces and flows in low Reynolds number hovering flight. *Two-dimensional computations vs robotic wing experiments*. *J Exp Biol*, 2004, 207: 449-460.
- [10] Pennycuic C J. Wingbeat frequency of birds in steady cruising flight. *New data and improved predictions*. *J Exp Biol*, 1996, 199: 1613-1618.
- [11] Ansari S A, Knowles K, Zbikowski R. Insect-like flapping wings in the hover. Part 1: *Effect of wing kinematics*. *J Aircraft*, 2008, 45: 1945-1954.
- [12] Wu J Z, Lu X Y, Zhuang L X. *Integral force acting on a body due to local flow structures*. *J Fluid Mech*, 2007, 576: 265-286.
- [13] Wu C J, Wang L. *Numerical simulations of self-propelled swimming of 3D bionic fish school*. *Sci China Ser E-Tech Sci*, 2009, 52: 658-669.

## Contact Author Email Address

cjwudut@dlut.edu.cn

## Copyright Statement

The authors confirm that they, and/or their company or organization, hold copyright on all of the original material included in this paper. The authors also confirm that they have obtained permission, from the copyright holder of any third party material included in this paper, to publish it as part of their paper. The authors confirm that they give permission, or have obtained permission from the copyright holder of this paper, for the publication and distribution of this paper as part of the ICAS 2014 proceedings or as individual off-prints from the proceedings.